ROYAL SOCIETY OF CHEMISTRY

PAPER

Check for updates

Active MOF water harvester with extraordinary productivity enabled by cooling-enhanced sorption†

Yaohui Feng, Lurong Ge, Yao Zhao, Qian Li, Ruzhu Wang [ID] and Tianshu Ge [ID] *

Extracting water from the air using a metal–organic framework (MOF) is an emerging solution to mitigate the global water crisis. Reported MOF water harvesters have improved water productivity from 0.1, 1.0 to 3.5 L_{H_2O} kg_{MOF}^{-1} d^{-1} using different strategies, but still cannot meet practical demands. Herein, we report the design of a MOF water harvester with tunable sorption–desorption behaviors by introducing cooling-assisted adsorption. Triple benefits brought by cooling effects—rapid sorption, enhanced capacity and reduced desorption temperature—deliver extraordinary productivities of 7.75–22.81 L_{H_2O} kg_{MOF}^{-1} d^{-1} in a diverse range of climates (10–35 °C, 20–80%RH), outperforming the best-performing MOF water harvester. Field tests produced 990.4 mL of clean water continuously throughout the day using a heat pump-integrated harvester in weather with an extremely low RH of 26%, corresponding to a productivity of 9.9 L_{H_2O} kg_{MOF}^{-1} d^{-1} with an energy consumption of 2.96 kW h $L_{H_2O}^{-1}$, demonstrating the great potential to provide adequate drinking water in real-world scenarios.

Broader context

The escalating global water scarcity motivates people to find innovative water solutions to quench the world's thirst. Sorption-based atmospheric water harvesting (SAWH) is a promising technology due to its wide climate adaptivity. However, the low water productivity and high energy consumption of current water harvesters underestimated the great potential of SAWH at an engineering scale owing to the weakened heat and mass transfer when scaling up materials-based SAWH. Here, we report an active and continuous water harvester using a metal–organic framework by introducing cooling in the sorption stage, enabling rapid dynamics, low-temperature regeneration, and high-water productivity. Applied cooling helps SAWH broaden the climate adaptivity, making water harvesting possible even if the ambient humidity is beyond the intrinsic boundary of materials. An innovative heat pump-integrated device with compact adsorber designs demonstrated impressive water production at the liter scale in a semi-arid climate, which could provide a feasible solution for practical water harvesting in a real-world application.

Introduction

The water crisis is a pressing challenge of the current era, impacting the two-thirds of the world's population who struggle with water scarcity.[1,2] With only about 2.5% of the water source on the earth being from freshwater sources, population growth, climate change, and water pollution have further exacerbated water consumption and thus threatened global sustainable development.[3,4] The severe water crisis and urgent demands from the economic, public health, and national security sectors call for accessible, clean, and safe drinking water.[5,6] Emerging

Engineering Research Center of Solar Power & Refrigeration (MOE), Institute of Refrigeration and Cryogenics, Shanghai Jiao Tong University, Shanghai 200240, China. E-mail: baby_wo@sjtu.edu.cn

† Electronic supplementary information (ESI) available. See DOI: https://doi.org/10.1039/d3ee03134a

solar stills for desalination provide an excellent solution with continuously improving efficiency,[7–9] but their dependence on water sources limits their development in remote inland areas. In this context, sorption-based atmospheric water harvesting (SAWH), which extracts water from the atmosphere, presents a unique pathway to the provision of clean water in arid regions and has great potential to solve the water problem for one billion people.[10] By employing sorbents with an abundant porous structure, moisture can be trapped in the pores and then converted into liquid water by the thermal-driven desorption and ambient-driven dewing processes.[11,12]

As early as the last century, the desire for drinking water has inspired the construction of SAWH devices, but their further development was impeded by the lack of ideal sorbents.[13] Encouragingly, the emergence of metal–organic frameworks (MOFs) with high hydrolytic stability, superior sorption capacity and tailorable structure has recently revitalized interest in

This journal is © The Royal Society of Chemistry 2024

Energy Environ. Sci., 2024, **17**, 1083–1094 | 1083

SAWH.[14–17] In 2017, the first conceptual SAWH was developed to yield water droplets using MOF-801 under arid conditions, demonstrating the feasibility of harvesting water from desert climates.[18] This breakthrough led to extensive research on producing practical water at an enlarged scale.[19] Primely, the monocyclic and passive SAWH is the main configuration adopted (Fig. S1A, ESI†).[20,21] A pioneering device was demonstrated to produce a daily water productivity of ~ 0.1 L_{H_2O} kg_{MOF}^{-1} (10–40%RH) in a desert climate using a few hundred grams of MOF-801.[22] However, the potential for even higher productivity needs to be unlocked.

One of the critical bottlenecks behind this low efficiency is limited water harvesting cycles. Optimizing moisture diffusion channels *via* pore design at the molecular level is a promising method for achieving rapid sorption–desorption dynamics.[23–25] In this regard, the concept of an active/ratcheting mode with multicyclic water harvesting has become feasible (Fig. S1B, ESI†).[26] With sorption during daytime and correspondingly increased harvesting cycles, productivity could be dramatically improved. Nevertheless, with the scaling-up of SAWH, an attenuation of the sorption rate is inevitable owing to worsened mass transfer. Practices have revealed that speeding up the sorption rate through forced convective airflow is more realistic and effective on an engineering scale.[27] This method has been successful in improving the daily water productivity to ~ 1.0 L_{H_2O} kg_{MOF}^{-1} (27 °C/32%RH) using MOF-303 in a multicyclic SAWH, leading to a nearly tenfold increase (Fig. S1C, ESI†).[28] Subsequently, the development of an adaptive mode with optimal sorption–desorption duration resulted in an impressive enhancement (3.5 L_{H_2O} kg_{MOF}^{-1} d^{-1} at 19–46%RH).[29] However, improving productivity still needs more attempts by maximizing the number of water-harvesting cycles and minimizing energy consumption. Moreover, existing MOF water harvesters employ multiple trays to load the MOF powders, which presents a challenge in terms of portability and compactness for practical needs. For instance, producing abundant drinking water for a person (at least 4 L of water) requires more than 1.14 kg of MOF, which corresponds to a sorbent unit size of *ca.* 0.15 m³.

Due to the complex interplay among adsorption, desorption, and condensation, each process needs to be carefully designed.[30] At the adsorption stage, sorbent selection is crucial to achieving a high sorption capacity. Microporous MOFs, such as MOF-801 and MOF-303, exhibit outstanding working capacities of *ca.* 0.3–0.4 g g⁻¹ in arid climates and have been successfully implemented in desert regions.[20,22,28,29] But the desorption becomes challenging under high air temperatures (T_a) or humid conditions.[31] In previous field tests, heating temperatures of up to 120 °C were required to achieve acceptable productivity.[28] Additionally, past harvesters have utilized an extra refrigeration-based system to lower the condensation temperature (T_{cd}, below 10 °C) to ensure condensation efficiency,[28,29] resulting in significant energy waste (approximately half of the total power consumption was used for condensation), which is inefficient from an energy utilization standpoint.

In this work, we report a design for a MOF water harvester by cooling-enhanced sorption to achieve a daily water productivity of 7.75–22.81 L_{H_2O} kg_{MOF}^{-1} d^{-1} under a wide range of climates (10–35 °C, 20–80%RH), which presents a great improvement compared with existing state-of-the-art active MOF water harvesters. The MIL-101(Cr) is shaped on two identical high-surface-to-volume heat exchangers with a high load density of 25.8 kg m⁻³. By controlling the cooling or heating temperature (T_c and T_h, referring to temperatures of supplied fluid), the sorption or desorption behaviors can be tuned due to the changed air temperature and humidity gradient near the sorbent. Two independent sorbent units undergo sorption and desorption in turn, allowing a sorbent unit of 0.007–0.02 m³ to continuously deliver 4 L of water. By tuning the sorption behavior *via* cooling assistance, the working zone can be extended to an arid climate at as low as 20%RH, even though the intrinsic operational RH of MIL-101(Cr) needs to be higher than 45%. By re-utilizing the cooling energy from the adsorption stage to desorption, the T_h could be reduced to as low as 45 °C. With compactness, cooling effect and convective airflow, the sorption period of the MOF adsorber could be shortened to within 20 minutes. A practical test in a real-world scenario with an extremely low RH of 26% resulted in the collection of nearly 1 L of water during one day, with a corresponding productivity of 9.9 L_{H_2O} kg_{MOF}^{-1} d^{-1} and a competitive energy consumption of 2.96 kW h $L_{H_2O}^{-1}$. Water quality analysis confirmed that the produced water met WHO guidelines and China's national drinking standard.

Results and discussion

Basic principle of tunable sorption–desorption behaviors

Fig. 1A delineates the traditional criteria for sorbent selection in SAWH. Monocyclic SAWH takes advantage of diurnal weather fluctuations, and thus requires sorbents with suitable steps. For multicyclic SAWH, sorbents possessing low step pressure are appropriate, considering the extremely low humidity in the daytime. Previous works have shown great progress in multicyclic SAWH with improved productivity, while our thermodynamic analysis reveals that the microporous MOFs (*e.g.*, MOF-303 and MOF-801) with a step at low pressure exhibit high energic requirements (see Note S1, ESI†).

Following the similar principle of natural air temperature drop and RH rising from day to night, introducing active cooling at the adsorption stage could elevate the effective RH near the sorbents,[32] which provides an opportunity for the use of an energy-efficient mesoporous MOF (normally with a step at high pressure) in various climates. A promising MIL-101(Cr) with moderate step pressure and high water uptake is suitable for tuning the sorption behavior with cooling assistance (Note S1, ESI†). Once the MOF encounters arid weather, introducing cooling makes the isotherms shift to the low pressure (or humidity) zone and ensures effective operation. As indicated by the variable-temperature isotherms in Fig. 1B, with a decrease in sorption temperature, the isotherms could be tailored to low-pressure regions. If the humidity is beyond the operating humidity range in the daytime (RH < step RH), active cooling helps the sorbent capture moisture effectively
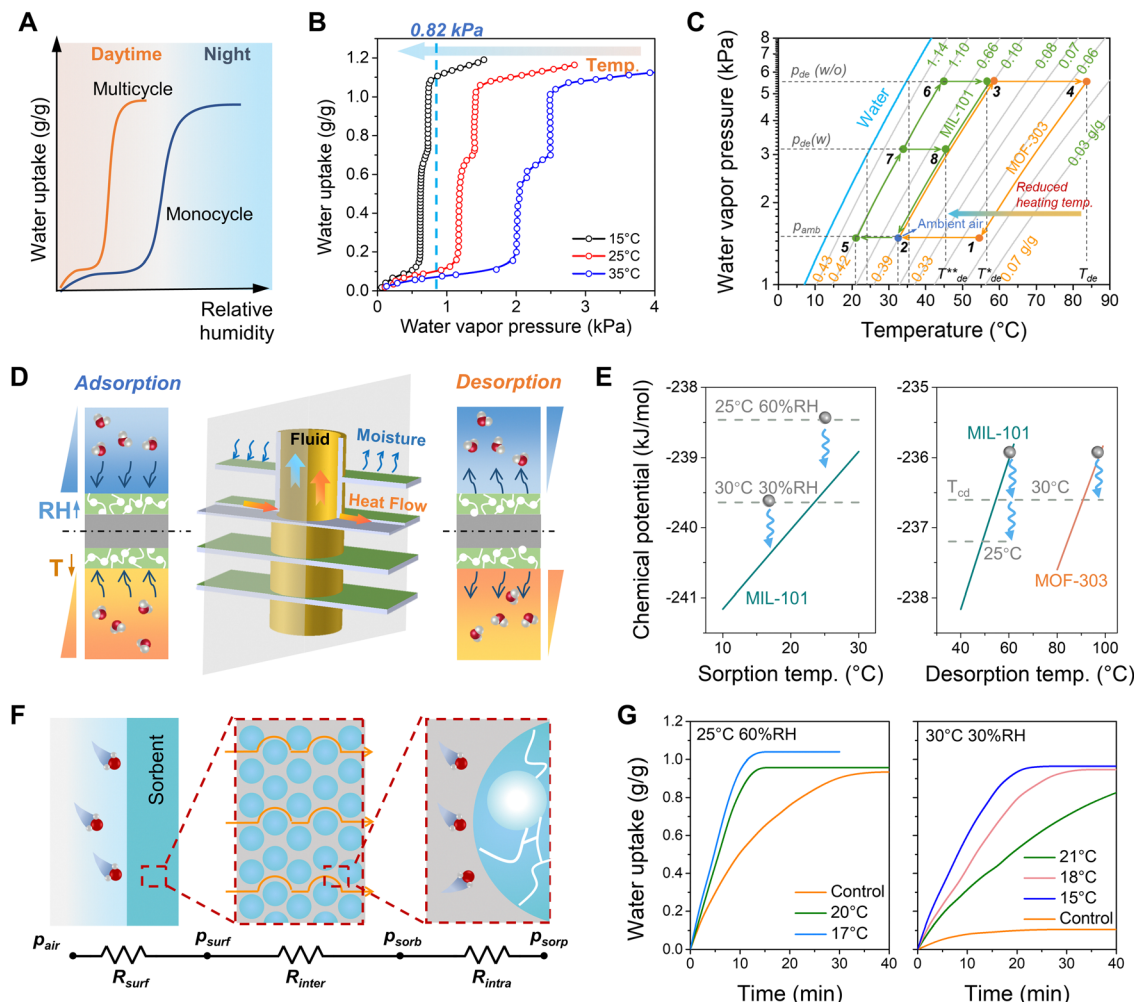
1084 | *Energy Environ. Sci.*, 2024, **17**, 1083–1094

This journal is © The Royal Society of Chemistry 2024

Fig. 1 Basic principle of tunable sorption–desorption behaviors. (A) The sorbent selection criterion of SAWH. (B) Isotherms of MIL-101(Cr) with different temperatures. (C) Water harvesting cycle in a lnp-T diagram. The green and orange lines refer to cycles using MIL-101 and MOF-303, respectively. p_{amb}, $p_{de}(w)$ and $p_{de}(w/o)$ represent the water vapor pressure of ambient air, desorption with cooling method and desorption without cooling method, respectively. (D) Temperature and humidity gradients at the interface of air and sorbent. (E) Explanation from the view of chemical potential. The chemical potential of the sorbent could be calculated by the sorption/desorption temperature and pressure. 40%RH and 35%RH is used to calculate the chemical potential of sorption and desorption pressure for MIL-101, respectively. 10%RH is used to determine the chemical potential of MOF-303 at the desorption stage. The T_{cd} refers to the condensation temperature. (F) Mass transfer resistance network of sorption stage. The R_{surf}, R_{inter}, and R_{intra} represent the mass transfer resistance of the surface, inter-crystalline and intra-crystalline diffusion, respectively. p_{air}, p_{surf}, and p_{sorb} refer to the water vapor pressure of ambient air, the surface of sorbent, pore of sorbent, respectively. The p_{sorp} means the sorption equilibrium pressure. (G) Dynamic sorption tests using a MOF coating sample with and without cooling.

(Fig. S2–S4, ESI†). The step point at 15 °C mitigates to a zone where the humidity is lower than 5 g kg^{-1} dry air (0.82 kPa), covering almost all regions in the world. This means using a sorption temperature of 15 °C could adapt to most climates.

Fig. 1C depicts the lnp-T diagram of the water harvesting cycle using MIL-101 (the cycle with MOF-303 represents traditional SAWH). Due to the high-pressure step position of MIL-101, the water harvesting cycle (2–5–6–3) could be driven by a lower temperature (T^*_{de}) than that using MOF-303 (cycle 1–2–3–4 at T_{de}). Additionally, if the waste cooling energy from the adsorption stage is utilized to lower the condensation temperature, desorption temperature is expected to be further reduced (from T^*_{de} to T^{**}_{de}), leading to a water harvesting cycle described as 2–5–7–8. Using this principle, the basic configuration of the

proposed SAWH can be illuminated in Fig. S5 (ESI†), where adsorption and desorption occur with the cooling and heating supply, meanwhile, the sorption heat can be eliminated by the cooling effect, and extra cooling energy could be recovered to the condenser.

Considering the required cooling/heating operations, the compact heat exchanger is selected for constructing the harvester owing to its high heat/mass transfer efficiency. The reforming temperature and humidity gradients at the interface between air and sorbent break the constraint of ambient conditions, allowing effective moisture sorption and release (see Fig. 1D and Fig. S6, ESI†). The explanation from the view of chemical potential revealed that cooling effect contributes the significant driving force for sorption and desorption (Fig. 1E, and Note S2,

This journal is © The Royal Society of Chemistry 2024

Energy Environ. Sci., 2024, **17**, 1083–1094 | **1085**

ESI†). The mass transfer resistance network indicated that the bulk parameters (dimension and convective airflow) can also contribute to the fast dynamics as well as the material design for optimized intrinsic kinetics (*e.g.*, porosity and tortuosity) (Fig. 1F and Note S3, ESI†). The dynamics experiments using a MOF sample proved the above theoretical analysis, resulting in a faster sorption rate and higher capacity with cooling effect than that of the control case without cooling (Fig. 1G), which provides an opportunity for increasing the number of water-harvesting cycles to maximize daily productivity. It should be noted that, although cooling is introduced, the cooling is only required to trigger the sorption behavior, thus the T_c is still higher than the dew point to maintain an energy-efficient process.

To fabricate this tunable MOF water harvester, we first synthesized MIL-101(Cr) (see the Experimental section) and then shaped it onto compact heat exchangers (210 × 205 × 45 mm) *via* an instantaneous-evaporation spraying method (Fig. S7–S9, ESI†). The high-temperature medium warrants instant evaporation of MOF solution, resulting in a stable and uniform sorbent layer on the metal surface (Fig. S10, ESI†). Compared with traditional acrylic trays (0.2 W m^{-1} K^{-1}), the high thermal conductivities of the aluminum fin (217 W m^{-1} K^{-1}) and copper pipe (379 W m^{-1} K^{-1}) provide a better heat transfer path. Considering the thermal resistance of the MOF coating, the thickness of MOF was controlled to within *ca.* 300 μm (Fig. S11, ESI†). The high surface-to-volume ratio (*ca.* 516 m^2 m^{-3}) meets the demands of compactness for a portable and scalable SAWH in most scenarios. A dynamics comparison between the coating sample and powders also

proved that the coating method will relatively promote the sorption rate owing to the enlarged contact surface and reduced mass transfer path (Fig. S12, ESI†), which also could be explained by the mass transfer network with reduced inter-crystalline diffusion resistance (Fig. 1F).

Performance evaluation of tunable SAWH in mild weather

Device fabrication. To maximize water production, it is imperative to undertake continuous cooling and heating operations (Fig. S1D, ESI†). To this end, we engineered a MOF water harvester using two identical adsorbers that alternate between sorption and desorption, and assembled an air-cooled condenser to exchange the air flows of adsorption and desorption (Fig. 2A). Once the sorption and desorption reach equilibrium, two switchable air ducts work to exchange the role of adsorber and desorber (Fig. 2B), and the water valves are used to change the flow direction of internal fluid, allowing continuous water production (see the detailed constructions in Fig. S13–S17 and the Experimental section, ESI†). The 100 g MOFs were loaded onto the two heat exchangers as the adsorber and desorber. The corresponding loading density was *ca.* 25.8 kg m^{-3}, which is three-fold higher than the reported tray-style sorbent unit (7.8 kg m^{-3}).[29] During our exploration periods, the MOFs underwent more than 3000 sorption–desorption cycles. The well-maintained powder XRD patterns and isotherms before and after cycling proved the stability of the synthesized MOF, and the simulated vibration and strong airflow revealed the stability of shaping methods (Fig. S18–S20, ESI†).
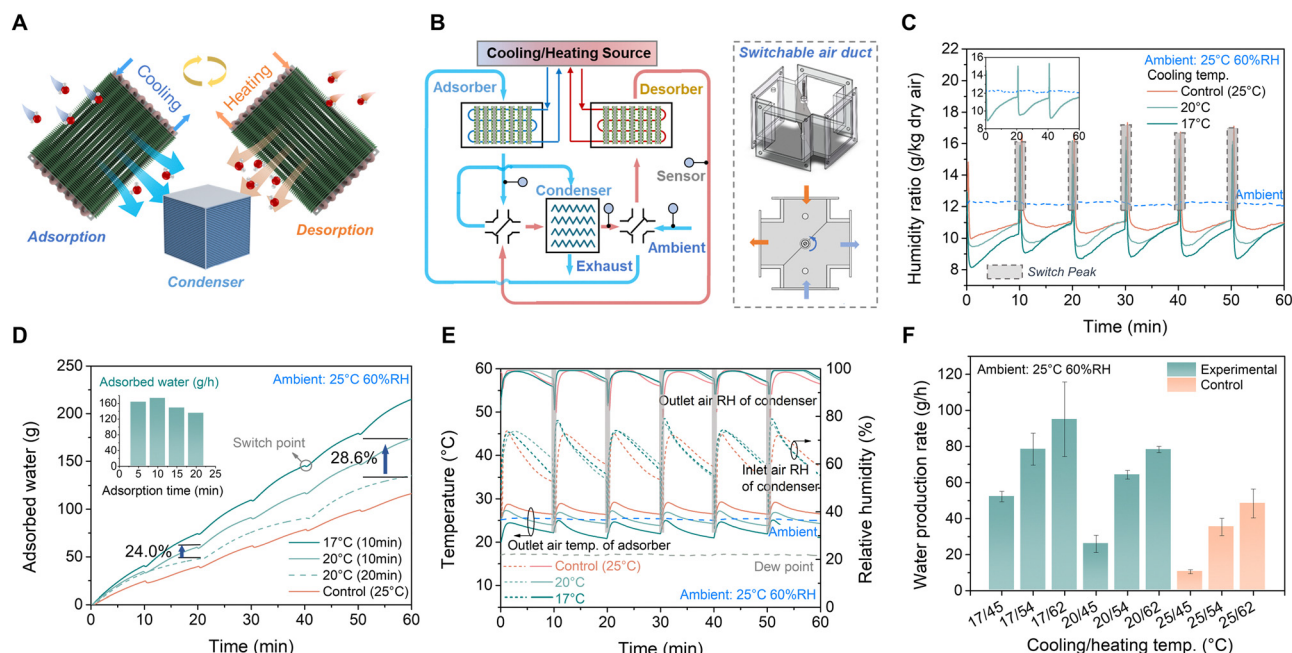

Fig. 2 Water harvesting performance in 25 °C/60%RH. (A) Configurations of the MOF water harvester. (B) Device design of the MOF water harvester. The sorption and desorption airflows can be exchanged by two switchable air ducts. (C) Typical dynamic sorption curves with different cooling temperatures. The humidity ratio refers to the outlet air of the adsorber. (D) Mass variation of adsorbed water. (E) Evolution of temperature and humidity in the condenser. (F) Water production rate with different cooling and heating temperatures. The error bars represent the mean ± s.d. and the data are determined by the results of six sorption–desorption cycles.

1086 | *Energy Environ. Sci.*, 2024, **17**, 1083–1094

This journal is © The Royal Society of Chemistry 2024

Sorption. For MIL-101, the normal operational weather zone falls in the region where the humidity is above 45% RH (Fig. S3, ESI†). We firstly tested the sorption and desorption performance under typical mild ambient conditions of 25 °C/60% RH. The humidity changes of the outlet air in the adsorber are recorded in Fig. 2C. A control case was carried out by keeping cooling temperature (T_c) the same as the ambient air temperature (T_a). Arising from the mixture of two airflows, each switching operation using the four-way air valve causes the peaks, as marked in grey in Fig. 2C (about 3 seconds, see Fig. S18, ESI†). In Fig. 2C, the area of the absolute humidity (humidity ratio, g kg^{-1} dry air) difference between the ambient and outlet air of the adsorber indicates the quality of captured moisture by the sorbent unit (Note S4, ESI†). It is found that with decreasing T_c from 25 to 20 and then to 17 °C, the adsorption capacity at the same duration is improved, indicating that the sorption dynamics are promoted, which is consistent with the sample test (Fig. 1G). The dynamics results reveal that although the mass of sorbent used in a MOF adsorber is 10 000 times larger than that used in the sorption analyzer (*ca.* 1–10 mg), the sorption kinetics still has no attenuation (Fig. S21, ESI†). Such a method provides a promising fabrication way towards a commercial SAWH with a fast water-harvesting cycle.

Prolonging the adsorption time to 20 minutes, the outlet air humidity tends toward ambient humidity over time (see the inset graph in Fig. 2C), indicating that the sorption reaches equilibrium at about 20 minutes. Such rapid dynamic sorption benefits from synergistic impacts of the external convective airflow and high humidity difference caused by the cooling effect (Fig. 1G). To quantify the effects of convective airflow and cooling effect, a comparison case was conducted using the same MOF adsorber with natural airflow. The mass transfer resistance analysis revealed that introducing convective airflow promotes the sorption rate by 87%, and the cooling effect will further bring 63.3 to 109.8% improvement of the sorption rate (see Note S3, ESI†). Despite that, the long duration of sorption leads to the loss of desorption due to the unequal sorption/desorption rate. The transient mass change of adsorbed water with different switching durations reveals that using an optimal duration of 10 minutes could improve the overall quality of the adsorbed water (Fig. 2D). After two sorption periods, the mass of adsorbed water is 24% more than that using a longer sorption time (20 minutes), and the enhancement will be cumulated to 28.6% after a one-hour sorption–desorption process. According to the mass of adsorbed water per hour, the sorption period of 10 minutes is appropriate (Fig. 2D).

Desorption. At the desorption stage, the released moisture flows into the condenser to form liquid water. As shown in Fig. 2E, after the switching operation, the outlet air RH of the condenser reaches 100% and then decreases over time, and the inlet air RH shows a decreasing trend, indicating that desorption and condensation processes are ongoing and last around 10 minutes. Compared with the control case, the outlet air temperature of the adsorber is lower than the ambient temperature, and thus the extra cooling energy is conducive to condensation. When the T_c is kept at 20 °C, the outlet air

temperature is first higher than the T_a attributed from the mixture of heating and cooling fluid during the switchover, and then lower than the T_a. However, using cooling water at 17 °C will overcome this negative effect. The mass of adsorbed and released water indicates that the harvester could be driven by the low-temperature source of 45 °C, but a higher T_h could provide more adsorber or released water (Fig. S20, ESI†).

Condensation. Regarding practical water production, the control case only produces 10.46 g, 35.38 g, and 48.47 g of water per hour when T_h is 45 °C, 54 °C and 62 °C, respectively (Fig. 2F). By comparison, the maximum water production rate can reach up to 95.5 g h^{-1} with cooling assistance, which is nearly 96.1% higher than the control case at T_h of 62 °C. This enhancement is more remarkable for low-temperature driven SAWH. The production rate using T_c of 17 °C is 399% and 122% higher than the control case with T_h of 45 °C and 54 °C, respectively. The temperature decrease of 3 °C (T_c from 20 °C to 17 °C) contributes to a 100% improvement in water production rate when T_h is 45 °C, while this enhancement is weakened at a higher heating temperature (with ∼20% enhancement when T_h is 54 °C or 62 °C) since the higher temperatures need better thermal management to avoid the heat loss to the environment.

Feasibility validation of water harvesting in arid climate

Naturally, climate fluctuations always exist, and thus the feasibility of using MIL-101 in arid climates needs to be validated. Different from the results under mild humidity conditions (RH > 45%), the sorption capacity in an arid climate depends heavily on the cooling effect (Fig. S2 and Note S2, ESI†). It is only when the when T_c is reduced to a critical temperature that the effective local RH near the sorbent allows more moisture to be captured. Here, we test the water harvesting performance in a typical arid climate (30 °C/30%RH). As shown in Fig. 3A, the adsorbed water per cycle within 10 minutes is 8.25 g when T_c is 21 °C, occupying only 19% of the maximum sorption capacity. The weak heat transfer hinders the mass transfer, and thus the improvement of the adsorption capacity is limited. When T_c is reduced to 18 °C and 15 °C, the masses of adsorbed water are 16.04 g and 21.33 g, respectively, with corresponding sorption capacities of 38.2% and 50.8%. Also, experiencing a longer sorption duration helps improve the capacity by keeping the sorbent temperature near the cooling temperature and caused higher effective RH. When the sorption duration is prolonged to 20 minutes, the adsorbed water reaches nearly 97.7% of its maximum capacity (see Fig. 3B), which also proved that cooling-assisted sorption is effective in an arid climate using MIL-101. The trade-off effect calls for further discussion about the sorption period and cooling temperature in arid climates.

To find the optimal switch point, we calculated the dynamic sorption and desorption curves, indicating that although a longer sorption time is conducive to higher sorption capacity per cycle, there is no significant increase in the sorption rate per hour (see Fig. 3C). The results also prove that the heat transfer is fast and the mass transfer is not delayed thanks to the thin sorbent layer. However, from the desorption view, it is
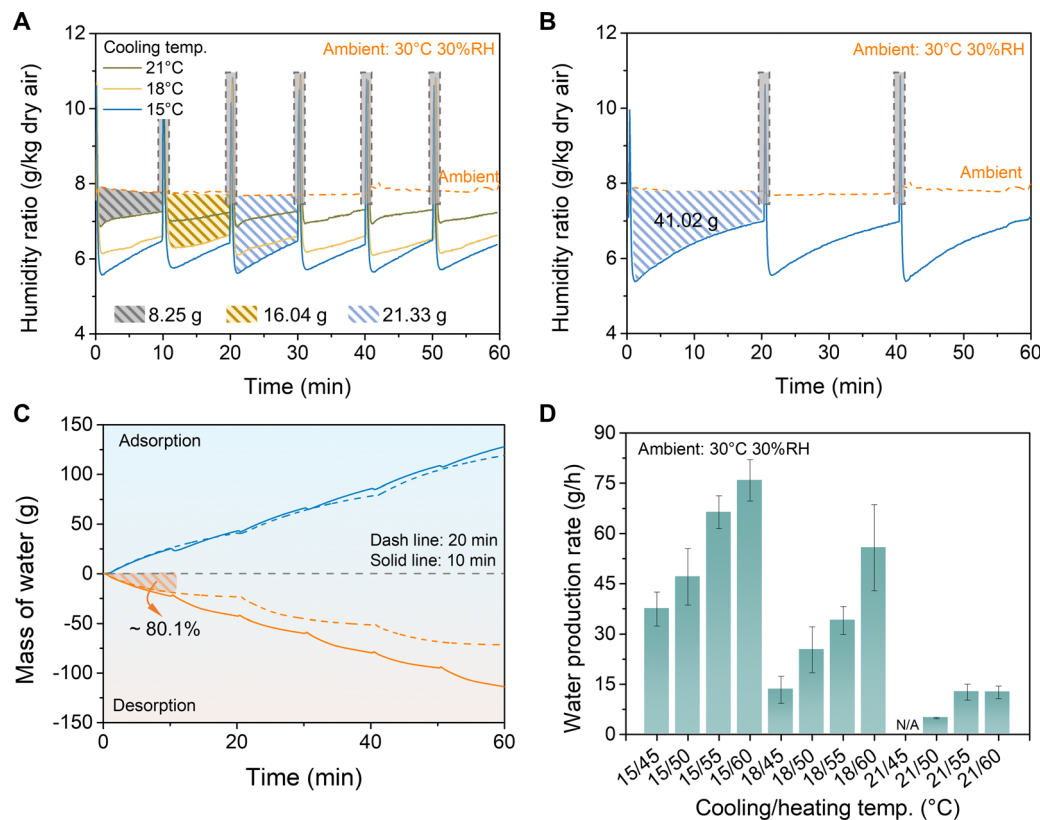
This journal is © The Royal Society of Chemistry 2024

Energy Environ. Sci., 2024, **17**, 1083–1094 | **1087**

Fig. 3 Feasibility of water harvesting in an arid climate (30 °C 30%RH). (A) Typical dynamic sorption curves of outlet air for an adsorber with different cooling temperatures. (B) Dynamic sorption curves with a sorption duration of 20 minutes. (C) Mass change of adsorbed water or released water with different sorption durations. (D) Water production rate with different cooling and heating temperatures. The error bars represent the mean ± s.d. and the data are determined from the results of six sorption–desorption cycles.

worth noting that dynamic desorption curves reveal that the desorbed water within 10 minutes accesses almost 80.1% of the total desorbed water within 20 minutes (Fig. 3C). In this case, the shorter sorption–desorption time will benefit the rapid desorption, thereby improving the cumulative released water. After the one-hour sorption–desorption cycle, the cumulative mass of desorbed water using a switching frequency of 10 minutes is 59.3% higher than that using 20 minutes.

The desorption behaviors are conducted by tuning the heating temperature, revealing that a low temperature of 50 °C is also sufficient to release water (Fig. S22, ESI†). With a T_c of 15 °C, when the T_h is higher than 45 °C, the release efficiency is improved up to 0.7–0.8, and the adsorbed or released water no longer shows a strong correlation with the temperature. This desorption process driven by small temperature differences provides a great potential to utilize low-grade thermal energy.

For conventional water collection without tuning, this device cannot produce liquid water under this arid climate since the ambient RH is beyond its working zone. With the cooling tuning, the promoted local RH allows for collecting water. As shown in Fig. 3D, a maximum water production rate of 75.87 g h^{-1} is accessible at 15/60 °C (T_c/T_h). The temperature decreases of 3 °C (from 18 °C to 15 °C) contribute 36.0%, 94.9%, 86.0% and 179.8% increase in the production rate when T_h is 60 °C, 55 °C, 50 °C and 45 °C, respectively. But no water is

collected under the conditions of 21/45 °C due to the tiny temperature difference between sorption and desorption. With a relatively higher cooling temperature, the resistance of heat conductivity weakens the cooling effect, and the higher cooling temperature also refers to the higher condensation temperature, making the requirement for a heating source tougher.

Global water production potential

As revealed above, compared with the control case, introducing the cooling effect will improve the mass of condensate water. Such evidence also indicates that cooling-assisted sorption enhances the sorption capacity and dynamics, regardless of the environment, whether it is mild or arid climates. After investigations under the representative climate zones, we aim to explore the practical potential of water production using this fabricated harvester on a global scale.

We firstly collected annual average climates in 188 main global cities, as shown in Fig. 4A (detailed locations in Fig. S23, ESI†). Based on the sorption properties of MIL-101, the water harvester can effectively function in the region with RH > 45%, covering *ca.* 86% of global regions. In other weather zones, the tunable operation strategy permits this harvester to work effectively. According to the tuning principle with cooling/heating operations, the critical cooling temperature should enable sorption by keeping the local humidity near the sorbent
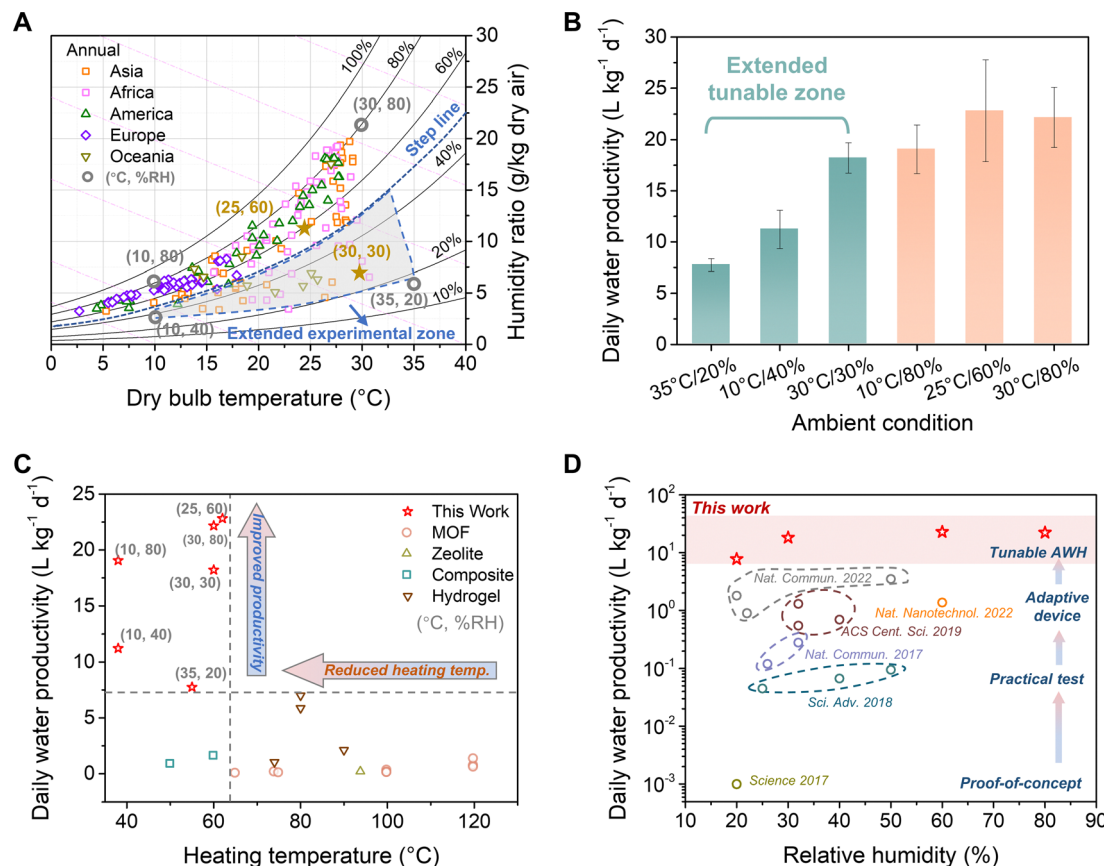
1088 | *Energy Environ. Sci.*, 2024, **17**, 1083–1094

This journal is © The Royal Society of Chemistry 2024

Fig. 4 Water production in various climates. (A) Annual average weather data in the main global cities. (B) Daily water productivity in different climates. (C) Comparison of water productivity and heating temperature between this work and reported works. (D) Comparison of water productivity between this work and reported MOF water harvester. The error bars represent the mean ± s.d. and the data are determined from the results of six sorption–desorption cycles. Note that the water productivity in ref. 18 was cited from ref. 36.

higher than the upper limit of step RH range in the isotherm, and the critical heating temperature should trigger the desorption by maintaining local humidity lower than the lower limit of its step RH range (Note S5, ESI†). With the critical cooling/heating temperatures, we tested the performance in the boundary climate marked in Fig. 4A to investigate the feasibility of extended weather zones, as shown in Fig. 4B. As revealed, the daily water productivity can be up to *ca.* 22.81 L_{H_2O} kg_{MOF}^{-1} d^{-1} at 25 °C/60%RH and 22.16 L_{H_2O} kg_{MOF}^{-1} d^{-1} at 30 °C/80%RH (also see Fig. S24, ESI†). A slight reduction in productivity can be found in the cold-humid region (10 °C/80%RH) since the cold temperature weakens the movement of water molecules, but the productivity remains at 19.06 L_{H_2O} kg_{MOF}^{-1} d^{-1}. In the extended climate zone, the daily productivities are 7.75, 11.22, and 18.21 L_{H_2O} kg_{MOF}^{-1} d^{-1} under hot-arid (35 °C/20%RH), cold-arid (10 °C/40%RH) and typical arid (30 °C/30%RH) climates, respectively. The relatively low productivity in the hot-arid region is caused by the greater heat transfer resistance and limited cooling capacity in the test rig. However, such harsh environments have relatively short duration in a given year due to diurnal and seasonal weather fluctuation.

Featured with tunable behaviors, both reduced heating temperature and improved productivity can be achieved simultaneously, as presented in Fig. 4C. Benefiting from the designed operation mode, the water production performance of this device is superior to that of devices in the reported literature.[12,21,25,28,33–35] Particularly, we summarized the development of MOF water harvesters[18,20,22,23,28,29,36] (Fig. 4D). Initially, the conceptual harvester is only validated with nearly no liquid water. Since then, great strides have been made from 0.1 to 1 L_{H_2O} kg_{MOF}^{-1} d^{-1} (32%RH), and even up to 3.5 L_{H_2O} kg_{MOF}^{-1} d^{-1} (19–46%RH). In this work, the triple bonus brought by the cooling effect—rapid dynamics, enhanced sorption capacity and reduced heating temperature—contributes to a high production yield and an improvement of one order of magnitude.

Considering that the reported active SAWH used electricity to drive water production, we demonstrated the comparison of energy consumption between reported works and our design driven by an electric heat pump. The cooling and heating could be supplied simultaneously by the evaporation and condensation process, and the energy consumption of the compressor is determined based on the cooling and heating capacity. The comparison reveals that energy-efficient SAWH can be achieved by our design (Fig. S25 and Table S3, ESI†), and the comparison with the direct dewing method indicates the energy consumption

This journal is © The Royal Society of Chemistry 2024

Energy Environ. Sci., 2024, **17**, 1083–1094 | **1089**

of our design is competitive and the harvester has wide climate adaptivity (Fig. S26, ESI†).

Practical water production using heat pump-integrated SAWH

With precisely controlled temperatures and stable environments, the water harvester works in an ideal state. For moving towards practical application, energy consumption should be taken into consideration. As discussed above, considering the working principle of the inverse Carnot cycle of a heat pump, carrying heat from a low-temperature heat sink to a high-temperature heat source, energy-efficient water production is expected. We then integrated a heat pump into the harvester to provide the cooling and heating energy simultaneously and alone by replacing the water baths used in the indoor test. One of the operation processes is shown in Fig. 5A. When an electricity-driven compressor operates, the refrigerant is condensed to release heat in the condenser and evaporated to absorb heat in the evaporator. Two plate heat exchangers (refrigerant to water) act as a heat transfer medium to transport the heat to the MOF adsorber and desorber (Fig. S27 and S28, ESI†). By switching the four-way valve in the water loop and exchanging airflows using the same switchable air ducts in the indoor test (Fig. 2B), the adsorption and desorption can be exchanged continuously to produce freshwater (see the Experimental section). The practical heat pump-driven harvester is shown in Fig. 5B.

We demonstrated this all-in-one harvester in a real-world scenario in Shanghai, China (30°40′ N, 120°52′ E). The typical weather during an experimental day was recorded in Fig. 5C. The RH was 50–65% at night with an extremely low RH of 26% in the daytime. The ambient temperature was 22–25 °C at night and rose to 36 °C during the daytime. When the device worked,

the T_c and T_h were controlled at 17 °C and 50 °C at high humidity conditions. With the ambient temperature raising, the cooling temperature was slightly increased to 19 °C, and the heating temperature was correspondingly increased to 53 °C (see Fig. S29 and S30, ESI†). During the test process, the outlet RH of the condenser remained near 100%, indicating the water condensation lasted all the time (see Fig. S31–S34, ESI†). We recorded the quality of collected water every hour, as shown in Fig. 5D (details in Table S4, ESI†). The water production rate was fast at night and became low in the daytime. Despite the ultra-low temperature driven SAWH, remarkably, 990.41 mL of liquid water was collected and the total power consumption was *ca.* 122 W (including 14 W for air fans and 12 W for pumps), the corresponding specific power consumption was 2.96 kW h $L_{H_2O}^{-1}$ and daily water productivity was 9.9 L_{H_2O} kg_{MOF}^{-1} d^{-1} (26–65%RH), which was 2.82 times that of an advanced MOF-based water harvester (3.5 L_{H_2O} kg_{MOF}^{-1} d^{-1}, 19–46%RH).[29] Considering the electricity price is around $0.08 kW h^{-1}, the related price for producing 1 L water is about $0.24 based on this field test (see Note S6 and Table S5–S6, ESI†).

As a comparison, we summarized the performance of state-of-the-art active MOF water harvesters in Table 1. The feasibility of water harvesting under a broad range of weather conditions has been proven in this work, and the rapid sorption–desorption cycles enable a superior water yield per kg MOF per day with low power consumption, even if air cooling is employed. Different from reported works that used an electrical heater and refrigerator to drive the respective desorption and condensation, a single heat pump was used here to supply cooling and heating simultaneously. High productivity and a well-designed MOF adsorber ensure a compact sorbent unit
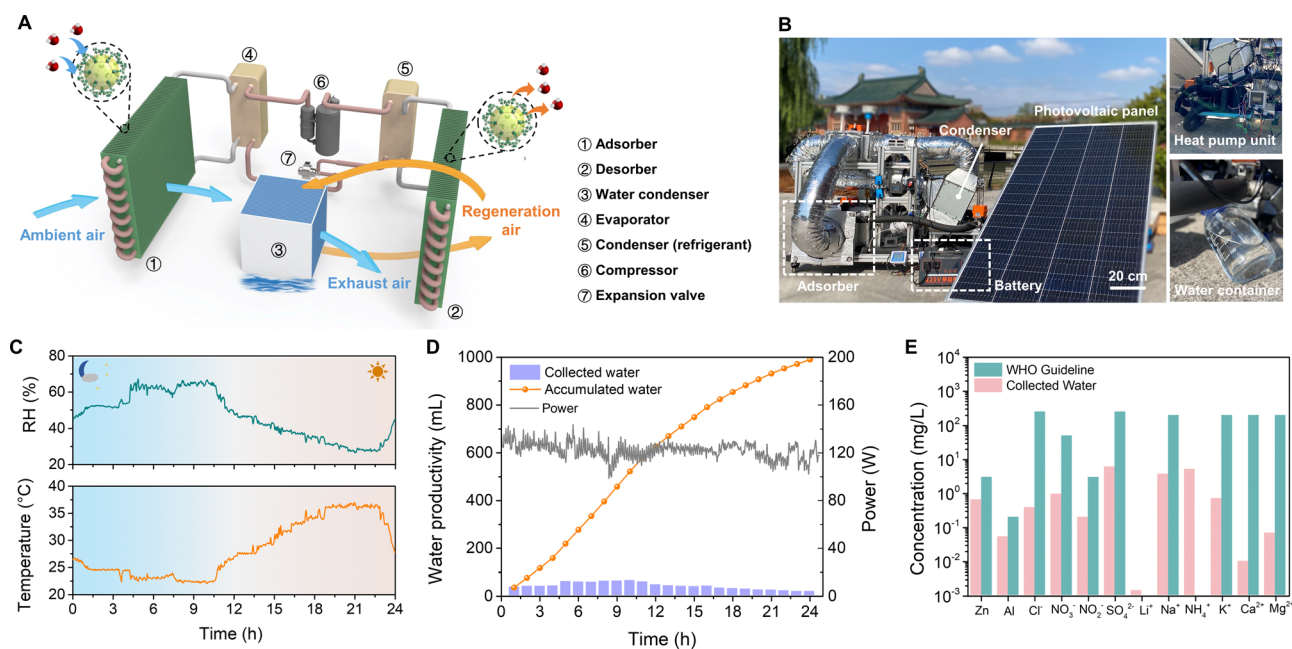

Fig. 5 Practical test using heat pump-integrated SAWH. (A) Principal illumination of heat pump-driven MOF water harvester. (B) Practical image of the device. (C) Recorded weather data in an experimental day. (D) Mass of collected water and cumulated water. (E) The concentration of metals and ions in the collected water.

1090 | *Energy Environ. Sci.,* 2024, **17**, 1083–1094

This journal is © The Royal Society of Chemistry 2024

Table 1 Comparison with active MOF water harvesters

Sorbent	Proven conditions	Equilibrium sorption time (h)	Productivity (L kg^{-1} d^{-1})	Size of sorbent unit for 4 L d^{-1} (m^3)	Energy (kW h L^{-1})	Continuous or not	Energy supply		Ref.
							Desorption	Condensation	
MIL-101	10–35 °C 20–80%RH	0.33	7.78–22.8	0.007–0.02	2.96^a	√	Heat pump	Air cooling	This work
MOF-801	19–46%RH	0.5–0.67	1.8–3.5	0.15–0.28	1.67–5.25^b	×	Electrical heater	Refrigerator	29
MOF-801	15–35 °C 10–70%RH	0.67	1.2–2.4	0.21–0.43	3–7^b	×	Electrical heater	Refrigerator	29
MOF-303	10–32%RH	0.8–2.2	0.7–1.3	0.05–0.07	5.33^a	×	Electrical heater	Refrigerator	28

^{a} Based on the practical test. ^{b} Depends on the environments.

of 0.016 m^3 (based on a field test) when producing 4 L water per day, which makes this harvester more attractive than other reported devices. For the active harvester, the auxiliary equipment is also important, which always covers a large area or volume. Almost all the reported active harvesters have no optimized system configurations in the experiments, which leads to an unfair comparison for the whole size. As indicated in Fig. S35 (ESI†), the optimized SAWH could reduce total volume by 89.4%. In this case, our comparisons only calculated the sorbent unit since this is the core part of a harvester. The comprehensive comparisons of materials-, sorbent unit-, and device-level are also conducted in Tables S7 and S8 (ESI†). It should be noted that the demonstration of heat pump-integrated SAWH in the field test employed a mini-compressor with low COP (coefficient of performance, standard COP is lower than 2.2 based on the product guideline). When scaling up this harvester with more synthesized MOF, a commercial high-efficiency compressor with a high COP can be used (the commercial compressor has a high COP of 5–6),[37–39] bringing a great potential to reduce power consumption by at least 56% (ca. 1.3 kW h L^{-1}), which shows the competitive potential for a commercial dewing harvester (5.6 kW h L^{-1} in arid conditions and 2.52 kW h L^{-1} in mild conditions[40]). More importantly, our demonstrations provide a paradigm for commercialization using low-temperature driving, validating a flexible strategy to adapt to various kinds of weather.

We finally measured the concentration of metals and ions in the collected water (Fig. 5E). The details of this can be found in Table S9 and S10 (ESI†). Although a chromium-based MOF is used, chromium cannot be detected in the collected water owing to its superior stability, as well as other hazardous metals, showing the water quality can meet the WHO guidelines and national drinking standards of China (GB 5749-2022). However, mineral elements are also lacking. A suitable concentration of these elements (e.g., sodium, potassium and calcium) is beneficial to health. In this case, the mineralization process should be supplemented for drinking water.

Outlook

Cooling source

We believe that this fabrication and operation mode could stimulate further investigations into how to choose a better cooling source to achieve higher productivity. Besides the demonstration using a heat pump in this work, recent emerging radiative cooling also gives inspiration as a cooling source to be integrated in a fully passive AWH.[41,42] In addition, solid-state cooling technologies (e.g., thermoelectric and caloric-based cooling) provide a feasible strategy for portable or personal devises for AWH.[32,43] Toward a building application, the cooling source also could be supplied by an air-conditioning system to provide a low-carbon footprint.[44]

Sorbent selection

Not limited to MIL-101, the tuning method is also applicable to other sorbents. The key point for sorbent selection depends on the consideration of climates and operation modes. Since weather changes with time and location, microporous MOFs or COFs (e.g., MOF-801 and MOF-303) are suitable in an extremely arid climate,[45] and hydrogel is promising in stable humid environments.[46,47] But the sorbents with moderate step pressure (e.g., MIL-101) are more suitable for the regions with humidity and temperature changes by a wide margin. In addition, the emerging strategies of preventing salt leakage has made salt-based composites a promising choice.[48–50] However, compared with traditional SAWH, no matter what sorbent is selected, the feasible zone of a specific sorbent will be extended with cooling assistance in the adsorption stage. Meanwhile, although cooling is introduced, the evaporation temperature is still higher than the dew point (Fig. S36, ESI†), resulting in the potential of energy-efficient SAWH and wide climate adaptivity compared with the commercial dewing method (Fig. S37, ESI†).

Cost and thermal design

The cost analysis in this work indicated that the AWH holds significant promise to provide a clean water supply. Although the cost of MOFs would be a concern for water harvesters, the large-scale and green synthesis provides a promising way for scalable implementation of AWH.[51] With a greater amount of synthesized MOF, direct heat exchange using a refrigerant as a medium could be employed, promising a lower power consumption. Considering the low thermal conductivity of MOFs, a better thermal design with highly efficient heat transfer technologies could be another important direction for enhancing heat transfer, such as employing a microchannel heat exchanger or shaping MOF with additive high thermal conductivity materials.

Conclusions

In summary, we report a design for a tunable MOF-based water harvester. By tuning the sorption–desorption behaviors with a

This journal is © The Royal Society of Chemistry 2024

Energy Environ. Sci., 2024, **17**, 1083–1094 | **1091**

cooling effect, the dynamics, sorption capacity and desorption temperature can be effectively controlled. We fabricated MOF adsorbers on compact heat exchangers and constructed an architecture for continuous freshwater production. Benefiting from the tunable behaviors, daily water productivity can reach 7.7–22.8 L_{H_2O} kg_{MOF}^{-1} d^{-1} from arid to humid weather (10–35 °C, 20–80%RH) with a low desorption temperature of 45–60 °C. The field test was carried out by integrating a heat pump to drive the water harvester, and an exceptionally high yield of 9.9 L_{H_2O} kg_{MOF}^{-1} d^{-1} was reached, which is superior to that of the reported best-performing MOF water harvester. Such a significant improvement has a clear benefit for practical applications. If 4 L of water is produced, the required MOF mass is only 0.18–0.52 kg (the reported harvester needs 1.1–5.7 kg), and the adsorber with a high surface-to-volume ratio permits using only 0.007–0.02 m^3 of the sorbent size. A competitive energy cost (2.96 kW h $L_{H_2O}^{-1}$) would inspire further investigations about this SAWH when turning to the commercial market.

We believe our demonstration of a MOF water harvester is an encouraging way to realize a better energy utilization pathway. Together with the efforts on sorbent tailoring, device fabrication and operation strategy from different discipline backgrounds, SAWH will promote a sustainable water supply in the future.

Experimental section

Materials synthesis

MIL-101(Cr) nanoparticles were synthesized based on a reported procedure with minor modifications.[52] Specifically, 1 mmol of chromic chloride hexahydrate and 1 mmol of terephthalic acid was dissolved into 7.2 mL of water. Subsequently, the mixed solution was vigorously stirred for complete dissolution before hydrothermal treatment at 190 °C for 24 h. After the reaction finished, the resultant solution was naturally cooled down to room temperature, and the recrystallized terephthalic acid was removed by low-speed centrifugation (1000 rpm, 3 min). Next, the MIL-101(Cr) product in the green color supernatant was collected by centrifugation (5000 rpm, 10 min), and washed with DMF and ethanol respectively.

Characterizations of materials

The morphologies of MIL-101(Cr) were characterized by a field emission scanning electron microscope (Sirion 200, FEI) and transmission electron microscope (TALOS F200X). The nitrogen adsorption of synthesized MIL-101(Cr) was measured by the volumetric method using the physisorption apparatus (Autosorb-IQ3, Quantachrome) at 77 K followed by the evacuated degas at 393 K for 12 h. The specific surface area is determined to be 3624.921 m^2 g^{-1} based on the Brunauer–Emmett–Teller (BET) method. Water vapor isotherms were measured by the physisorption apparatus (Belsorp Max, Microtrac BEL) at different temperatures. The powder X-ray diffraction (PXRD) pattern was measured by a multi-functional X-ray diffractometer (D8 Advance Da Vinci, Bruker). The concentrations of metal

elements and ions are detected by inductively coupled plasma-optical emission spectroscopy (ICP-OES, Avio 500) and ion chromatography (ICS-5000+/900). The thermal diffusivity was tested by the laser flash method (LFA 467, Netzsch, GER).

Shaping method of MOF coating

The synthesized MOF solution was collected several times and then was mixed with ethanol with a volume ratio of 1 : 5. The mixture was stirred vigorously for 30 min and experienced an ultrasonic treatment for 10 min to form a uniform solution. About 15%wt vinyl acetate was added to the mixture as the binder. The final mixture was stirred continuously to obtain suitable viscosity.

The bare heat exchangers (HX) were immersed with commercial scouring powder to clean the oil and impurities on the surface and then dried at 70 °C. Before shaping, the cycling hot water of 60 °C was introduced into the pipe of the heat exchanger to heat the surface of the heat exchanger. The mixture solution was sprayed on the surface of the heat exchanger. When the solution reached the hot surface, the solvent was evaporated to form a uniform MOF layer. The above spraying operation was repeated several times. Too thick coating will increase the heat and mass transfer resistance but too thin coating will lead to a low sorption capacity. Based on the experience of the sorption cooling devices and the results of thermal conductivity, the thickness of sorbent coating is kept around 300 μm. Finally, the heat exchanger was dried at 70 °C for several hours until the water inside the heat exchanger was evaporated thoroughly. Then the mass change of the heat exchanger was recorded as shown in Table S1 (ESI†).

Water harvester construction

The MOF adsorbers were fabricated by spraying the MOF solution on the surface of heat exchangers (210 × 205 × 45 mm). Two switchable air ducts (Fig. 2B) were assembled by acrylic to connect the adsorber and air-cooled condenser (20 × 20 × 20 cm, fin spacing of 3 mm). Two adsorbers were placed within one of the switchable air ducts and linked to another switchable air duct (Fig. S13–S16, ESI†). The switch operations were controlled by actuators to drive the blades. Four sensors were placed to record the temperature and humidity at the inlet and outlet of the adsorbers and condenser (Fig. S16, ESI†). The air pipes were wrapped by thermal insulation and aluminum foil to prevent heat loss. The condenser was tilted to allow water droplets to drop onto the bottom of the condensation chamber *via* gravity, and a paper tissue was used to drive the water flow by capillarity to accelerate water collection (Fig. S17, ESI†). For the controlled temperature experiments in the lab, the cooling and heating temperatures were adjusted by two water baths, and two four-way valves were employed to switch the water flow.

For the field test of the water harvester, water temperatures were controlled by the heat pump unit (Fig. S27, ESI†), and the switchable air duct was the same as used in the lab test. A DC-24V compressor (cooling capacity of 100–500 W), two plate heat exchangers (54 × 119 × 50 mm) and a capillary tube (diameter

1092 | *Energy Environ. Sci.*, 2024, **17**, 1083–1094

This journal is © The Royal Society of Chemistry 2024

of 2 mm) were connected as a cooling/heating unit. Two sensors were used to record the evaporation and condensation pressure. When the heat pump worked, water was cooled or heated by the heat exchange with the refrigerant (R134a) in the evaporator and condenser, respectively. The PV-powered battery was used to supply the electricity in the field test.

Performance test of the MOF water harvester

The lab test of the MOF water harvester was carried out in a climate controlled room where humidity and temperature can be accurately adjusted. The cooling or heating temperature was controlled by two water baths. The airflow rates during sorption and desorption were set to 75 and 45 $m^3 h^{-1}$ to fit cooling and heating requirements and guarantee a practical condensation process (14 W with two air fans). Ambient temperature and humidity were recorded by the thermos/hygrometers (HygroFlex3) with an accuracy of ±0.3 °C and $\pm2\%$RH. The collected liquid water was recorded by the electronic balance (3 kg/0.01 g).

The field test was carried out in Shanghai Jiao Tong University, Shanghai, China (30°40′ N, 120°52′ E) in October 2022. The air temperature was changed from 22 to 37 °C, and humidity from 26 to 66%RH. Two MOF adsorbers were fabricated in the water harvester, and the total mass of MOF was 100 g. The field test was conducted from 16:00 to 16:00 the next day. The quality of collected water was weighted using an electronic balance (3 kg/0.01 g) every hour. The required electricity was from a battery (3.3 kW h), and the battery can be charged by a solar PV panel. When the test began, the compressor was run to provide the cooling and heating water, and the water flow was pumped by a DC-12V pump (max. power of 6 W). The switch was controlled by the electric relay (Delixi, JSS48A-S) and the switching frequency was set as 10 minutes. The total power consumption was also recorded on the power meter.

Author contributions

Y. F. and L. G. synthesized the sorbents. Y. F. shaped the MOF adsorber, fabricated the water harvester, carried out the experiments, and analyzed the experimental data. Y. Z. and Q. L. participated in the shakedown test of the heat pump unit. Y. F. prepared the manuscript. All authors contributed to the review and editing. R. W. and T. G. conceived the idea and led the project.

Conflicts of interest

There are no conflicts to declare.

Acknowledgements

References

1 P. Greve, T. Kahil, J. Mochizuki, T. Schinko, Y. Satoh, P. Burek, G. Fischer, S. Tramberend, R. Burtscher, S. Langan and Y. Wada, *Nat. Sustain.*, 2018, **1**, 486–494.

2 M. M. Mekonnen and A. Y. Hoekstra, *Sci. Adv.*, 2016, **2**, e1500323.

3 L. Zhang, Z. Xu, L. Zhao, B. Bhatia, Y. Zhong, S. Gong and E. N. Wang, *Energy Environ. Sci.*, 2021, **14**, 1771–1793.

4 Z. Yu, T. Zhu, J. Zhang, M. Ge, S. Fu and Y. Lai, *Adv. Funct. Mater.*, 2022, **32**, 2200359.

5 Y. Zhang and S. C. Tan, *Nat. Sustain.*, 2022, **5**, 554–556.

6 Z. Yu, J. Zhang, S. Li, Z. Zhou, Z. Qin, H. Liu, Y. Lai and S. Fu, *Adv. Funct. Mater.*, 2023, **33**, 2210730.

7 Y. Shi, R. Li, Y. Jin, S. Zhuo, L. Shi, J. Chang, S. Hong, K.-C. Ng and P. Wang, *Joule*, 2018, **2**, 1171–1186.

8 H. Shan, Z. Ye, J. Yu, R. Wang and Z. Xu, *Device*, 2023, **1**, 100065.

9 L. Zhang, X. Li, Y. Zhong, A. Leroy, Z. Xu, L. Zhao and E. N. Wang, *Nat. Commun.*, 2022, **13**, 849.

10 J. Lord, A. Thomas, N. Treat, M. Forkin, R. Bain, P. Dulac, C. H. Behroozi, T. Mamutov, J. Fongheiser, N. Kobilansky, S. Washburn, C. Truesdell, C. Lee and P. H. Schmaelzle, *Nature*, 2021, **598**, 611–617.

11 Y. Guo, W. Guan, C. Lei, H. Lu, W. Shi and G. Yu, *Nat. Commun.*, 2022, **13**, 2761.

12 H. Shan, C. Li, Z. Chen, W. Ying, P. Poredoš, Z. Ye, Q. Pan, J. Wang and R. Wang, *Nat. Commun.*, 2022, **13**, 5406.

13 Y. Tu, R. Wang, Y. Zhang and J. Wang, *Joule*, 2018, **2**, 1452–1475.

14 H. Lu, W. Shi, Y. Guo, W. Guan, C. Lei and G. Yu, *Adv. Mater.*, 2022, **34**, 2110079.

15 K. Yang, T. Pan, Q. Lei, X. Dong, Q. Cheng and Y. Han, *Environ. Sci. Technol.*, 2021, **55**, 6542–6560.

16 H. Furukawa, F. Gándara, Y.-B. Zhang, J. Jiang, W. L. Queen, M. R. Hudson and O. M. Yaghi, *J. Am. Chem. Soc.*, 2014, **136**, 4369–4381.

17 W. Shi, W. Guan, C. Lei and G. Yu, *Angew. Chem., Int. Ed.*, 2022, **61**, e202211267.

18 H. Kim, S. Yang, S. R. Rao, S. Narayanan, E. A. Kapustin, H. Furukawa, A. S. Umans, O. M. Yaghi and E. N. Wang, *Science*, 2017, **356**, 430–434.

19 N. Hanikel, M. S. Prévot and O. M. Yaghi, *Nat. Nanotechnol.*, 2020, **15**, 348–355.

20 H. Kim, S. R. Rao, E. A. Kapustin, L. Zhao, S. Yang, O. M. Yaghi and E. N. Wang, *Nat. Commun.*, 2018, **9**, 1191.

21 A. LaPotin, Y. Zhong, L. Zhang, L. Zhao, A. Leroy, H. Kim, S. R. Rao and E. N. Wang, *Joule*, 2021, **5**, 166–182.

This journal is © The Royal Society of Chemistry 2024

Energy Environ. Sci., 2024, **17**, 1083–1094 | 1093

22 F. Fathieh, M. J. Kalmutzki, E. A. Kapustin, P. J. Waller, J. Yang and O. M. Yaghi, *Sci. Adv.*, 2018, **4**, eaat3198.

23 Y. Song, N. Xu, G. Liu, H. Qi, W. Zhao, B. Zhu, L. Zhou and J. Zhu, *Nat. Nanotechnol.*, 2022, **17**, 857–863.

24 N. Hanikel, X. Pei, S. Chheda, H. Lyu, W. Jeong, J. Sauer, L. Gagliardi and O. M. Yaghi, *Science*, 2021, **374**, 454–459.

25 J. Xu, T. Li, T. Yan, S. Wu, M. Wu, J. Chao, X. Huo, P. Wang and R. Wang, *Energy Environ. Sci.*, 2021, **14**, 5979–5994.

26 H. Park, I. Haechler, G. Schnoering, M. D. Ponte, T. M. Schutzius and D. Poulikakos, *ACS Appl. Mater. Interfaces*, 2022, **14**, 2237–2245.

27 L. Hua, J. Xu and R. Wang, *Nano Energy*, 2021, **85**, 105977.

28 N. Hanikel, M. S. Prévot, F. Fathieh, E. A. Kapustin, H. Lyu, H. Wang, N. J. Diercks, T. G. Glover and O. M. Yaghi, *ACS Cent. Sci.*, 2019, **5**, 1699–1706.

29 H. A. Almassad, R. I. Abaza, L. Siwwan, B. Al-Maythalony and K. E. Cordova, *Nat. Commun.*, 2022, **13**, 4873.

30 Y. Feng, R. Wang and T. Ge, *Device*, 2023, **1**, 100054.

31 Y. Feng, R. Wang and T. Ge, *Adv. Sci.*, 2022, **9**, 2204508.

32 Y. Feng, T. Ge, B. Chen, G. Zhan and R. Wang, *Cell Rep. Phys. Sci.*, 2021, **2**, 100561.

33 R. Li, Y. Shi, M. Wu, S. Hong and P. Wang, *Nano Energy*, 2020, **67**, 104255.

34 H. Lu, W. Shi, J. H. Zhang, A. C. Chen, W. Guan, C. Lei, J. R. Greer, S. V. Boriskina and G. Yu, *Adv. Mater.*, 2022, **34**, 2205344.

35 C. Lei, Y. Guo, W. Guan, H. Lu, W. Shi and G. Yu, *Angew. Chem., Int. Ed.*, 2022, **61**, e202200271.

36 W. Xu and O. M. Yaghi, *ACS Cent. Sci.*, 2020, **6**, 1348–1354.

37 F. Schlosser, M. Jesper, J. Vogelsang, T. G. Walmsley, C. Arpagaus and J. Hesselbach, *Renewable Sustainable Energy Rev.*, 2020, **133**, 110219.

38 S. Garimella, K. Lockyear, D. Pharis, O. El Chawa, M. T. Hughes and G. Kini, *Joule*, 2022, **6**, 956–971.

39 B. Gido, E. Friedler and D. M. Broday, *Atmos. Res.*, 2016, **182**, 156–162.

40 F. Bagheri, *Water Resour. Ind.*, 2018, **20**, 23–28.

41 I. Haechler, H. Park, G. Schnoering, T. Gulich, M. Rohner, A. Tripathy, A. Milionis, T. M. Schutzius and D. Poulikakos, *Sci. Adv.*, 2021, **7**, eabf3978.

42 J. Li, X. Wang, D. Liang, N. Xu, B. Zhu, W. Li, P. Yao, Y. Jiang, X. Min, Z. Huang, S. Zhu, S. Fan and J. Zhu, *Sci. Adv.*, 2022, **8**, eabq0411.

43 X. Qian, D. Han, L. Zheng, J. Chen, M. Tyagi, Q. Li, F. Du, S. Zheng, X. Huang, S. Zhang, J. Shi, H. Huang, X. Shi, J. Chen, H. Qin, J. Bernholc, X. Chen, L.-Q. Chen, L. Hong and Q. M. Zhang, *Nature*, 2021, **600**, 664–669.

44 P. Poredoš, H. Shan and R. Wang, *Joule*, 2022, **6**, 1390–1393.

45 W. Song, Z. Zheng, A. H. Alawadhi and O. M. Yaghi, *Nat. Water*, 2023, **1**, 626–634.

46 W. Guan, Y. Zhao, C. Lei and G. Yu, *Proc. Natl. Acad. Sci. U. S. A.*, 2023, **120**, e2308969120.

47 W. Guan, C. Lei, Y. Guo, W. Shi and G. Yu, *Adv. Mater.*, 2022, 2207786.

48 Z. Yu, S. Li, J. Su, J. Zhang, D. Zhang, Z. Zhou, Z. Qin, X. Liu, Y. Lai and S. Fu, *Matter*, 2023, **6**, 3509–3525.

49 H. Shan, Q. Pan, C. Xiang, P. Poredoš, Q. Ma, Z. Ye, G. Hou and R. Wang, *Cell Rep. Phys. Sci.*, 2021, **2**, 100664.

50 H. Shan, P. Poredoš, Z. Ye, H. Qu, Y. Zhang, M. Zhou, R. Wang and S. C. Tan, *Adv. Mater.*, 2023, **35**, 2302038.

51 Z. Zheng, H. L. Nguyen, N. Hanikel, K. K.-Y. Li, Z. Zhou, T. Ma and O. M. Yaghi, *Nat. Protoc.*, 2023, **18**, 136–156.

52 M. Zhao, K. Yuan, Y. Wang, G. Li, J. Guo, L. Gu, W. Hu, H. Zhao and Z. Tang, *Nature*, 2016, **539**, 76–80.

1094 | *Energy Environ. Sci.*, 2024, **17**, 1083–1094

This journal is © The Royal Society of Chemistry 2024